J Solid State Electrochem (2011) 15:549–560
DOI 10.1007/s10008-010-1094-9

ORIGINAL PAPER

Fast protonic conductivity in crystalline benzenehexasulfonic acid hydrates

Evgeny M. Garanin · Yuriy V. Tolmachev · Scott D. Bunge · Anatoly K. Khitrin · Alexander N. Turanov · Andrey Malkovskiy · Alexei P. Sokolov

Received: 22 March 2010 / Revised: 30 April 2010 / Accepted: 4 May 2010 / Published online: 20 June 2010

Abstract We report on the crystal structures of two hydrates of benzenehexasulfonic acid, its water sorption isotherm, temperature- and humidity-dependent conductivity, along with ^{1}H NMR studies. At comparable humidities and temperatures, this *crystalline* material shows conductivity similar to Nafion, which conducts protons via *liquid* water channels. We believe that the presented discovery of fast protonic conductivity in benzenehexasulfonic acid at low humidities is encouraging for further efforts in developing highly sulfonated polymers as membranes for fuel cells.

Keywords Proton conductor · Fast protonic conductivity · Sulfonic acid · Humidity · Zundel ion · NMR

Introduction

The poor protonic conductivity of Nafion at humidities below 50% is one of the major impediments in the development of polymer electrolyte fuel cells for automotive applications [1–3]. In the case of Nafion and related materials, the problem stems from the fact that these materials rely on liquid water for proton transport and that the percolating water clusters disappear under lower humidity [4, 5]. It is believed that because of a large separation between sulfonic groups in Nafion, a direct proton transfer between them is not possible, and therefore, water plays the role of a proton carrier. The increase in the concentration of sulfonic groups may allow not only for the increase of conductivity at full hydration [6, 7] but also a higher conductivity at lower humidities. This was shown to be the case for sulfonated perfluoroalkyl polymers of different equivalent weights [6]. By sulfonation of a commercial polymer PEEK, Rikukawa and Sanui achieved the degree of sulfonation (DOS) of 0.3 SO_3H per aromatic ring with the resulting conductivity of 0.01 S/cm at 50% RH and 80°C [8]. Alberti et al. showed that for sulfonated PEEK, the conductivity at 75% RH and 100°C increases from 9×10^{-4} to 5×10^{-3} S/cm when the degree of sulfonation goes from 0.27 to 0.42 [9]. Tsuchida et al. claimed that the conductivity of polyphenylenesulfide increases over two orders of magnitude as the degree of sulfonation increases from 1.2 to 2.0 [10]. By polymerizing sulfonated monomers, Litt et al. produced polyphenylenes having one or two sulfonic acid group(s) per benzene ring. This materials showed impressive conductivities of 0.086 (DOS=1) and 0.45(DOS=2)S/cm at 50% RH and 0.01 (DOS=1) and 0.09 (DOS=2)S/cm at 15% RH and 75°C [11, 12]. Finally, we should mention the success of CsH_2PO_4 (with conductivity of 0.10 S/cm at 250°C and 0.30 atm water vapor pressure) [13] and related materials in intermediate-temperature fuel cells, although these materials do not allow for much room in terms of chemical modification and properties optimization.

Electronic supplementary material The online version of this article (doi:10.1007/s10008-010-1094-9) contains supplementary material, which is available to authorized users.

E. M. Garanin · Y. V. Tolmachev (✉) · S. D. Bunge · A. K. Khitrin
Department of Chemistry, Kent State University, Kent, OH 44242, USA
e-mail: ytolmach@kent.edu

A. N. Turanov
Zavoisky Physical-Technical Institute, Kazan 420029, Russia

A. Malkovskiy · A. P. Sokolov
Department of Polymer Science, The University of Akron, Akron OH44325, USA

In a recent review of possible routes toward low-humidity proton conducting membranes, Schuster et al. suggested "an inclusion of highly sulfonated systems with... small...–SO_3H separations into a future research" [5]. Inspired by these findings, we decided to investigate such a compound with a high concentration of and a small separation between sulfonic groups, which can serve as a prototype for a broad class of chemical compounds with adjustable structure and properties, i.e., benzenehexasulfonic acid (BHSA).

BHSA and its salts were synthesized in 1972 [14], and their reactivity [14], spectral [15], and electrochemical properties [16, 17] were investigated in the following years. The crystal structure of the hexasodium salt octahydrate was also determined [18, 19]. Neither the crystal structure nor the conductivity of benzenehexasulfonic acid has been reported previously.

Experimental section

Materials All commercially available reagents were used without further purification. Deionized water was used for aqueous reactions. 1,2,4,5-Tetrachlorobenzene was purchased from TCI America. Oleum (30%) and fuming HNO_3 were obtained from VWR International. Benzene, THF, 1,4-dioxane $CuSO_4 \times 5H_2O$, and Na_2SO_3 were obtained from Fisher Sci. DMSO-d_6, $CDCl_3$, and D_2O were purchased from Cambridge Isotope Laboratories.

1,4-Dinitrotetrachlorobenzene Oleum (30%) (225 g, 118 mL, 1.61 mol H_2SO_4 and 0.84 mol SO_3) was added dropwise under stirring to fuming nitric acid (225 g, 152 mL, 3.57 mol) in a 1,000-mL round-bottom flask. The reaction mixture was cooled down to room temperature, and 1,2,4,5-tetrachlorobenzene (32.4 g, 0.150 mol) was added. Reaction mixture was refluxed for 9 h under stirring. After cooling to room temperature, the mixture was poured onto ice (2 kg). A yellowish precipitate was filtered out and washed with cold water (300 mL). The crude was purified by recrystallization in 1,4-dioxane, resulting in white, needle-like crystals in 45% yield. ^{13}C NMR in $CDCl_3$: 149.5, 126.2 ppm; GC-MS: 306 (M^+); m.p. 232–233°C (lit.=233°C) [20]; IR (neat): 1,393.2, 1,546.4 cm^{-1}. GC-MS and ^1H NMR found no signals from 1,2,4,5-tetrachlorobenzene and 1,2,4,6-tetrachloronitrobenzene.

Sodium 2,3,5,6-tetrachlorobenzenedisulfonate dihydrate Solution of sodium sulfite (22.22 g, 176.3 mmol) in water (150 mL) was added dropwise to warm solution of 1,4-dinitrotetrachlorobenzene (5.44 g, 17.8 mmol) in 1,4-dioxane (75 mL) under stirring. The mixture was refluxed under stirring for 6 h. The solution was cooled to room temperature. The white precipitate formed over night was filtered, recrystallized from water, and dried in vacuum. Yield 38.5%. ^{13}C NMR in D_2O: 144.8, 135.7 ppm; ^{13}C NMR in DMSO-d_6: 144.9, 131.7 ppm. TGA: $-2H_2O$ at 100°C.

Sodium benzenehexasulfonate trihydrate (route 1) Disodium salt of tetrachloro-benzenedisulfonic acid dihydrate (6.840 g, 15.00 mmol), sodium sulfite (11.34 g, 9.000 mmol), water (60 mL), and $CuSO_4 \times 5H_2O$ (0.117 g, 0.468 mmol) were heated under reflux for 4 h. The precipitated white crystals of $Na_6BHSA \times 8H_2O$, formed upon cooling to room temperature, were filtered, washed with saturated solution of sodium chloride, and cold water, and dried in vacuo at 125°C. Yield 72%. ^{13}C NMR in D_2O: 151.9 ppm.

Sodium benzenehexasulfonate trihydrate (route 2) 1,4-Dinitrotetrachlorobenzene (6.20 g, 20.3 mmol) in 1,4-dioxane (40 mL) was added to aqueous solution of sodium sulfite (30.0 g, 238 mmol in 300 mL) and $CuSO_4 \times 5H_2O$ (0.094 g, 0.38 mmol). Reaction mixture was refluxed for 6 h. The precipitated white crystals of $Na_6BHSA \times 8H_2O$, formed upon cooling to room temperature, were filtered, washed with saturated solution of sodium chloride, and cold water, and dried in vacuo at 125°C. Yield 67%. ^{13}C NMR in D2O: 151.9 ppm.

Benzenehexasulfonic acid dodecahydrate A glass chromatographic column (inner diameter 2.5 cm, 67 cm length) was filled with 570 meq of cation-exchange resin (Amberlite IR-120H) (300 mL of wetted bed volume). The resin was converted into the H^+ form by flushing with 5.0 L of 6.05 M HCl (31 eq) followed by water rinsing. Sodium benzenehexasulfonate octahydrate (3.00 g, 4.06 mmol) was dissolved in water (700 mL) and passed through the ion exchange column followed by elution with water. The collected acidic solution (900 mL) was concentrated to 50 mL on rotary evaporator and passed through a second ion exchange column. The solution was evaporated at 22.5 torr pressure and 40°C to dryness. The powder was washed with THF till its color changed from brownish to white. Yield 96%. ^{13}C NMR in D2O: 151.9 ppm; isotopic pattern for electrospray ionization–ion trap mass spectrometry (ESI-MS) for $(M–H)^-$ (calcd/found): 557 Da (100%/100%), 558 Da (12%/13.8%), 559 Da (30.8%/31.5%); with a lower capillary voltage also 476 Da $(M–H–SO_3)^-$, 396 Da $(M–H–2SO_3)^-$, 278 Da $(M–2H)^{2-}$.

Chemical analyses

Gas chromatography–mass spectrometry (GC-MS) was performed with Finnigan Trace GC-2000/Polaris instrument

equipped with a Restek-5MS column (30 m long×0.25 mm ID fused silica coated with 0.5 μm 5%-diphenyl-95% polysiloxane) and an electron-impact ionization (70 eV) ion-trap mass analyzer set for positive ions. The injection port temperature was set at 250°C, the column temperature was held at 60°C for 2 min initially and then ramped to 250°C at 20°C/min and held there for 10 min. The temperatures of the GC-MS transfer line and of the ion source were maintained at 200 and 275°C, respectively. He carrier gas flow rate was 100 mL/min. One microliter of 1 mg/mL solution of analyte in acetonitrile was injected using the hot-needle technique with the split ratio of 100.

Flame emission spectroscopic analysis of Na was done with an Instrumentation Laboratory AA/AE spectrometer 157 after dissolving BHSA samples in water to make solutions with 10–15 mM concentration. Aqueous NaCl solutions (1–40 μM) were used as calibration standards.

Ion chromatography was used to measure the sulfate and chloride contents using a Dionex DX-100 apparatus equipped with an anion exchange column, an eluent suppressor column, and a conductivity detector. The samples were dissolved in water to yield the sulfate concentration in the range of 0.0125–0.125 μM and spiked with 0.05 μmol of $NaNO_3$ as an internal standard. $NaHCO_3$+3.5 mM Na_2CO_3 solution (1.0 mM) was used as an eluent. Solutions of Na_2SO_4 and NaCl were used as calibration standards.

ESI-MS was performed in the negative ion mode with Esquire-LC instrument (Hewlett Packard, Bruker) using direct injection of the analyte solution (18 μM benzenhexasulfonic acid+17 mM NH_4AcO+40% *v*/*v* acetonitrile in water) into the electrospray source at 100–250 μL/h flow rate. The ESI-MS parameters were as follows: nebulizer pressure 50 psi, dry gas flow rate 10 L/min, drying temperature 80°C, capillary voltage 4,500 V, end plate offset −750 V, skim1 −100 V, skim2 +2 V, cap exit offset −150 V, octopole −2.38 V, octopole RF 115.6 V, octopole delta −1.80 V, trap drive 53.7 V, lens1 5.0 V, lens2 90 V, multiplier 1,400 V, dynode 70 kV, cap exit 0 V, skimmer1 0 V, skimmer2 −300 V.

Other measurements: Elemental analysis was performed using Leco CHNS-932 instrument. FTIR spectra were obtained using Bruker Tensor 27 spectrometer with a single-reflection dome-shaped ZnSe ATR probe. Thermal gravimetric analysis was performed with TGA 2950 thermogravimetric analyzer. Melting points were determined using Nikon eclipse microscope model #E600POL equipped with a hot stage coupled with Mettler Toledo FP90 central processor unit.

X-ray diffraction To prepare single crystals, an aqueous solution of BHSA was evaporated to a syrup-like consistency on a rotary evaporator. Aliquots of the syrup were placed onto Petri dishes and left in desiccators under controlled humidity (9.5% and 33% maintained with KOH and $MgCl_2$ saturated salt solutions, respectively) for 5 days. The crystals obtained after drying under different humidities were used for crystallographic studies.

Single-crystal X-ray diffraction data were collected with a Bruker AXS diffractometer. The radiation used was graphite monochromatized Mo Kα radiation (λ=0.7107 Å). The sample crystal was mounted onto a thin glass fiber from a pool of Fluorolube™ and immediately placed under a stream of evaporating N_2. The lattice parameters were optimized from a least-squares calculation on carefully centered reflections. Lattice determination, data collection, structure refinement, scaling, and data reduction were carried out using APEX2 version 1.0-27 software package.

Each structure was solved using direct methods. This procedure yielded a number of the C, S, and O atoms. Subsequent Fourier synthesis yielded the remaining atom positions. The final refinement of each compound included anisotropic thermal parameters on all non-hydrogen atoms. X-ray crystallographic files in CIF format for the structures BHSA×14H_2O and BHSA×12H_2O are available from the Cambridge Data Base under CCDC 735435 and CCDC 735436, respectively.

Water sorption measurements The mass of absorbed and desorbed water as a function of relative humidity was measured using automatic instruments by Surface Measurement Systems Ltd. (Allentown, PA, USA) at 30°C and by Hiden Isochema (Warrington, UK) at 110°C.

Nuclear magnetic resonance ^{1}H and ^{13}C NMR spectra of liquid solutions were acquired with Bruker Avance 400 MHz spectrometer. NMR studies of powder samples (15 mm height in 5 mm OD tubes, equilibrated to the desired humidity at 20°C and sealed with a 1.0 mL air-filled headspace) were carried out with Varian Unity/Inova 500 MHz instrument at temperatures from 20 to 75°C. The samples were brought to the desired temperature within 5 min, held at this temperature for 5 min, measured for 5 min, and then cooled to 20°C within 5 min. The NMR peak areas were reproducible within 2%, suggesting that all changes in the sample upon temperature variations are fully reversible.

T_2 relaxation was studied using 90-τ–180°-τ echo sequence. Each echo (typical width 20 kHz) was averaged over four scans, and the spectra with 500-Hz Lorentzian broadening factors were integrated. T_1 relaxation was studied using 180°-τ–90° sequence. Proton diffusivity was measured using the Stejskal–Tanner pulsed-field-gradient sequence.

Conductivity The conductivity of powdered samples was measured as a function of temperature and humidity with a custom made four-point probe (inner electrode distance 5.00 mm, sample cylinder diameter 1.50 mm) in a porous zirconium phosphate cell, details of which are given in our previous report [21]. The cell was placed into an environmental chamber equipped with a humidity–temperature sensor, electrical feedthroughs, and gas inlet/outlet valves. The temperature of the chamber was controlled using a heating tape wrapped around it. At temperatures above 50°C, the humidity inside the chamber was controlled using a bubbler-type humidifier (Fideris, model FCTS BH) connected to the chamber via a heated line purged with He. At temperatures below 50°C, the humidity was maintained by saturated solutions of various salts placed inside the chamber. In order to get reproducible conductivity data (see Fig. S2), the powder loaded in the cell was caked first at 50–55% RH between 20 and 80°C till its conductivity raised to a constant value (usually 30 min). At this point, the sample was taken out the chamber, and the screws were tightened again. After this treatment, the specific conductivity values, at and below 85°C, became reproducible from sample to sample.

Impedance data were acquired with Solartron 1287 Electrochemical Interface and 1255B Frequency Response Analyzer using ZPlot software (Scribner Associates, Inc.). The frequency of the ac perturbation was step-scanned in logarithmic intervals in the region from 1 MHz to 0.1 Hz with a constant amplitude of 100 mV.

Results

Synthesis

Hexasodium salt of benzene hexasulfonic acid ($Na_6[C_6(SO_3)_6]$, Na6BHSA) was synthesized according to Refs. [14, 15] as shown in Scheme 1.

1,2,4,5-Tetrachlorodinitrobenzene (**A**) was synthesized by electrophilic aromatic nitration of commercially available 1,2,4,5-tetrachlorobenzene [20]. The nitration of electron deficient 1,2,4,5-tetrachlorobenzene was expectedly difficult and thus required harsh conditions. The reaction proceeds through formation of intermediate 1,2,4,5-tetrachloronitrobenzene, which can be easily detected by GC-MS and NMR spectroscopy. 1,2,4,5-Tetrachloronitrobenzene is also a major impurity in isolated crude **A**. Moderate yields of **A** can be attributed to the formation of benzene sulfonic acid derivatives, which can also be formed under similar conditions [22]. We further improved early reported procedure [20] by recrystallization of crude **A** in 1,4-dioxane.

Na_6BHSA can be made by two procedures: in two steps (route 1) or in a single step (route 2). Route 1 involves two districted steps: synthesis, isolation, and purification of sodium 2,3,5,6-tetrachlorobenzenedisulfonate (**B**) and Cu^{2+} catalyzed substitution of four –Cl of **B** on $–SO_3Na$ groups. While route 2 is essentially the same, it is a one pot procedure. Although one pot route gives higher isolated yields of Na_6BHSA in a time efficient manner, we chose to proceed with stepwise route because it yields more pure Na_6BHSA.

Prior to analysis, the salt was dried in a vacuum oven at 125°C to constant weight (8 h), purportedly yielding $Na_6BHSA\times3H_2O$ [14, 15]. The crude $Na_6BHSA\times3H_2O$ had a rather high sulfate content (sulfate/benzenehexasulfonate=8.1×10^{-2}mol/mol), probably due to oxidation of sulfite in air. Through a series of recrystallizations of the salt (as $Na_6BHSA\times8H_2O$) from water, samples with lower sulfate content were obtained. They were converted to BHSA using ion exchange resins. BHSA samples were dried at 20°C and 9.0% humidity to constant weight (48 h), resulting in $BHSA\times12H_2O$. Ion chromatography of these samples showed sulfate/benzenehexasulfonate molar ratios of 6.7×10^{-3}, 3.6×10^{-3}, and 8.1×10^{-4}mol/mol. The sodium/benzenhexasulfonate molar ratio for all BHSA samples was less than 2.24×10^{-4}mol/mol and chloride/benzenhexasulfonate molar ratio was less than 2.1×10^{-4}mol/mol. Unless specified otherwise, the data reported in this work refer to samples with 8.1×10^{-4}mol/mol $SO_4^{2-}/C_6(SO_3)_6^{6-}$ ratio.

Water sorption Prior to sorption measurements (Fig. 1), the samples were dried in vacuum at 130°C till constant weight (<1%/h change). Apparently, this process did not result in complete removal of water from $BHSA\times nH_2O$ powder since the plateaus in the water sorption isotherms (not shown) yielded values $n=9$ and 11 if $n=0$ is assumed after the drying. This finding contradicts the XRD that show the presence of crystals with $n=12$ and 14 (vide infra) at RH 9% and 33%, respectively. A better agreement between the sorption and XRD data is obtained if $n\sim2$–3 is assumed after drying (as shown in Fig. 1). This implies that before the sorption scans, the samples were mixtures of $BHSA\times4H_2O$ and dianhydride tetrahydrate (nominally, $BHSA\times2H_2O$) known from our separate TGA, NMR, and mass spectrometry studies [23]. It should be noted that drying at humidity over 1% at 30°C does not lead to n less than 11 (Fig. 1, triangles).

Crystal structure

We determined the XRD structures of three crystals at 100°K : **1** is $Na_6BHSA\times8H_2O$ $(C_6(SO_3^-)_6Na_6^+\times8H_2O$,

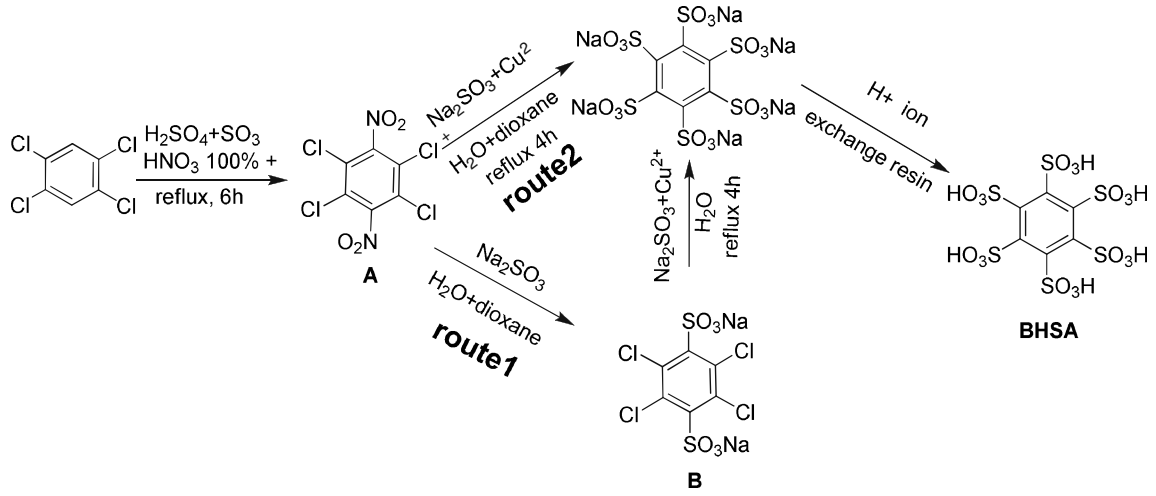

Scheme 1 Synthesis of benzenehexasulfonic acid (BHSA)

hexasodium octahydrate); **2** is BHSA×14H_2O ($C_6(SO_3^-)_6(H_3O^+)_6$×8H_2O, acid 14-hydrate, grown at 33.0% humidity); and **3** is BHSA×12H_2O ($C_6(SO_3^-)_6(H_3O^+)_6$×6H_2O, acid 12-hydrate, grown at 9.0% humidity). The room temperature powder X-ray diffractograms of BHSA×12H_2O and BHSA×14H_2O agree with the ones calculated from low temperature single-crystal XRD data, suggesting that no phase transitions occurred upon crystals cooling. In all cases, the structure of the benzenehexasulfonate is similar. The benzene ring possesses a shallow chair conformation (see Fig. 2) with C_{Ar}–C_{Ar}–C_{Ar}–C_{Ar}– torsion angles of 9.5°, 8.2°, and 9.1° for **1**, **2**, and **3**, respectively. C_{Ar}–C_{Ar} distances (CC) are elongated compared with benzene (0.1397 nm) and are 0.1408, 0.1405, and 0.1395 nm for **1**, **2**, and **3**, respectively. The substituent sulfonic groups alternate above and below the ring, with *S*–C_{Ar}–C_{Ar}–*S* torsion angles ranging from 42° to 44°. These findings are not surprising since similar distortions, which lower the steric repulsion between the substituent groups, have been reported in other hexasubstituted benzenes [19, 24].

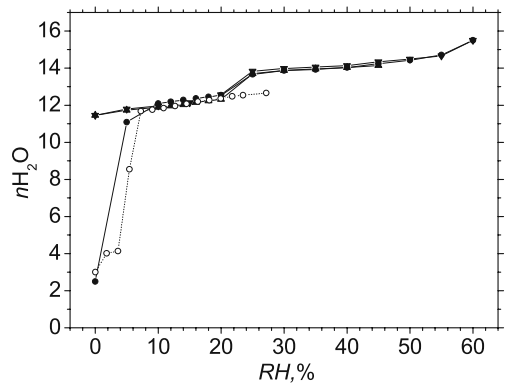

Fig. 1 Water sorption isotherms of BHSA at 30 (*solid lines*) and 110°C (*dotted line*). The samples were dried at 130°C, then the humidity was raised stepwise (*circles*), then lowered (*inverted triangles*), then raised again (*triangles*)

Despite stoichiometric similarity, **1** ($C_6(SO_3-)_6Na_6^+$×8H_2O) and **2** ($C_6(SO_3^-)_6(H_3O^+)_6$×8H_2O) have rather different structures. The latter (see Fig. 3) contains channels in the *c* direction filled with H_3O^+ ions hydrogen-bonded to H_2O molecules and sulfonate groups. Perpendicular to the *c* direction, there are (101) layers of benzenehexasulfonates separated by layers containing H_3O^+ and H_2O.

In contrast, the 1:1 hydronium/water stoichiometry in BHSA×12H_2O leads exclusively to formation of the Zundel ($H_5O_2^+$) ions. The latter have been identified in over 70 crystals, including four benzenesulfonate derivatives [25–28]. Since BHSA×12H_2O is the lower-humidity phase, we studied it in more details. A two-leveled layer of $H_5O_2^+$ cations separates layers formed by BHSA anions as shown in Fig. 4. The hydrogen bond in the Zundel ions is very strong, with the O–O distance being 0.240 nm, which is the smallest among Zundel ions in benzene sulfonate derivatives [25–28]. The broad peak at 3,150 cm^{-1} in the IR spectrum of BHSA×12H_2O, absent for BHSA×14H_2O, can be assigned to the strong hydrogen bond in Zundel ions [29] (Fig. 5).

According to low-temperature XRD (100 K), the closest distance between O atoms in Zundel ions and O atoms of sulfonic acid group are 0.274 nm for (O1) (O1–O3 distance) and 0.269 nm for O2 (O2–O4 distance), and the next closest distances between Zundel O atoms and O atoms of sulfonic groups are 0.290 nm (O1–O5 distance) and 0.291 nm (O2–O6 distance). On other hand, the room temperature infrared spectra of the two BHSA hydrates at 21°C show a complex structure of A band (Fig. 6) [30, 31]. Particularly, for BHSA×12H_2O, a main peak at 3,167 cm^{-1} and a shoulder at 3,342 cm^{-1} can be seen. The universal relationship between infrared OH stretching frequencies and O....O distances can be used to calculate O...O

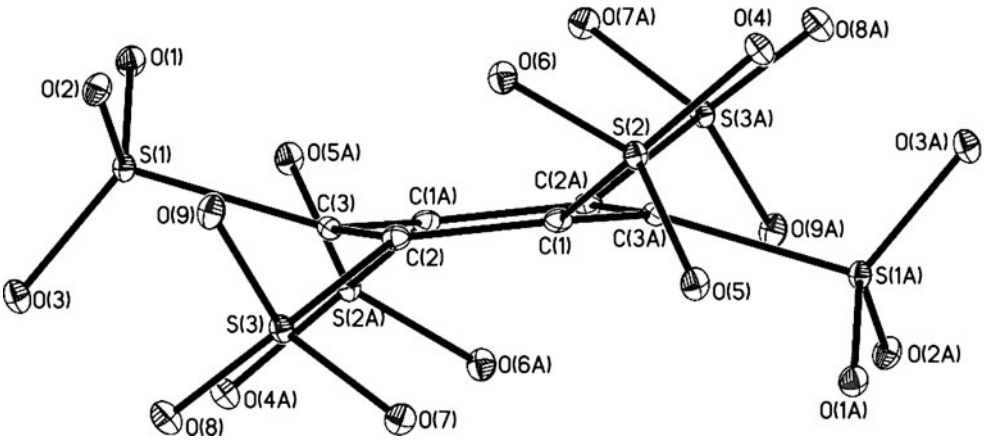

Fig. 2 Thermal ellipsoid plot of benzenehexasulfonate anion in BHSA×14H_2O. Ellipsoids are drawn at the 30% level

distances [32–38] (see Fig. 6). The calculated O...O distances are 0.29 and 0.27 nm and are in agreement with distances found from XRD data. Since both bands are pronounced in the infrared spectra, we believe that protons are disordered between O1–O3 and O1–O5 in one case and between O2–O4 and O2–O6 in another. Even if the disorder in the proton sublattice is not completely random, the longer O...O link at 0.290–0.291 nm is likely to play a key role in proton conduction in this material since an internal rotation of Zundel ion, moving H^+ between these positions, creates a pathway for interlayer proton transfer between sulfonic groups via an intermediate Zundel ion (Fig. 4). The third O...O shell around O atoms in the Zundel ions has an O atom from a $H_5O_2^+$ in a different layer at 0.3235 nm (Fig. 4) and an O atom from a sulfonate at 0.3280 nm (Fig. 4). Proton transfer over such distances requires rather large activation energies [34], but we cannot rule out this pathway without further studies (vide infra).

The $H_5O_2^+$ cations are arranged into hexameric clusters with no direct hydrogen bonds between Zundel cations within each cluster. Within a layer, the distance between two oxygen atoms of two closest Zundel cations of neighboring clusters is 0.431 nm. Clearly, this distance is too long for direct translocation of H^+ to occur. On the other hand, distances between O atoms of SO_3^- group and O atoms of Zundel cations are favorable for H^+ translocation (0.274 and 0.290 nm, respectively). Thus, proton can jump to O atom of sulfonic group and the SO_{3-} group can rotate around C–S bond delivering H^+ to neighboring cluster as shown in Fig. 4. The interlayer (within the *ab* plane) transport between Zundel cation hexamers requires rotation of a sulfonic group around a C–S bond, which is likely to be the rate-limiting step. The interlayer (in *c* direction) proton transport between the hexamers may occur more readily than the intralayer transport since the closest intralayer O...O distance between two neighboring clusters is smaller (0.3235 nm) than analogous interlayer O...O distance (0.431 nm). Within a cluster, the proton transport can occur by S–O bond rotation. This mechanism suggests that the intrinsic protonic conductivity of BHSA×12H_2O may be anisotropic.

In Raman spectra of BHSA at 21 °C (Fig. 7), a strong band at 1,064.4 cm^{-1} and a weaker band at 1,024.7 cm^{-1} correspond to benzene ring C–C vibrations, and a strong band at 1,118.3 cm^{-1} is due to a symmetric vibration of the SO_3 group [41]. A large difference between the two hydrates in the relative band intensities in the 400–1,200 cm^{-1} region agrees with the difference in the distortions of the $BHSA^{6-}$ anions in BHSA×14H_2O and BHSA×12H_2O inferred from the XRD data. The absence of a diffuse shoulder (soft modes) near the Rayleigh line, well known in other superionic phases and attributed to anion librations [42], indicates against a disorder in the O– sublattice.

Conductivity

The reproducible BHSA conductivity data were obtained only after caking the compressed powder at humidities over 50% as explained in the "Experimental" section and illustrated in Fig. S2 (Supporting information). The caking probably eliminates the effect of the intergrain and electrolyte–electrode contact resistances. The four-point impedance of BHSA shows purely ohmic behavior at low frequencies (the values of *ReZ* were used to calculate the specific conductivity). At kHz frequencies (see Fig. S1, Supporting information), a parallel capacitance shows up. The value of this capacitance (0.25–0.35 nF) does not change with the relative humidity; however, it is too large to be accounted for by the capacitance of the cell (estimated <1 pF), and therefore, we attribute this capacitance to grain boundaries in BHSA samples.

The dependence of the conductivity of BHSA powder on relative humidity at several temperatures is shown in Fig. 8. It is worth noting that sulfate content (see "Synthesis" section) affects the conductivity of BHSA significantly, e.g., the conductivity of samples with 6.7×10^{-3}mol/mol sulfate/BHSA (open blue circles) is five to 10 times larger

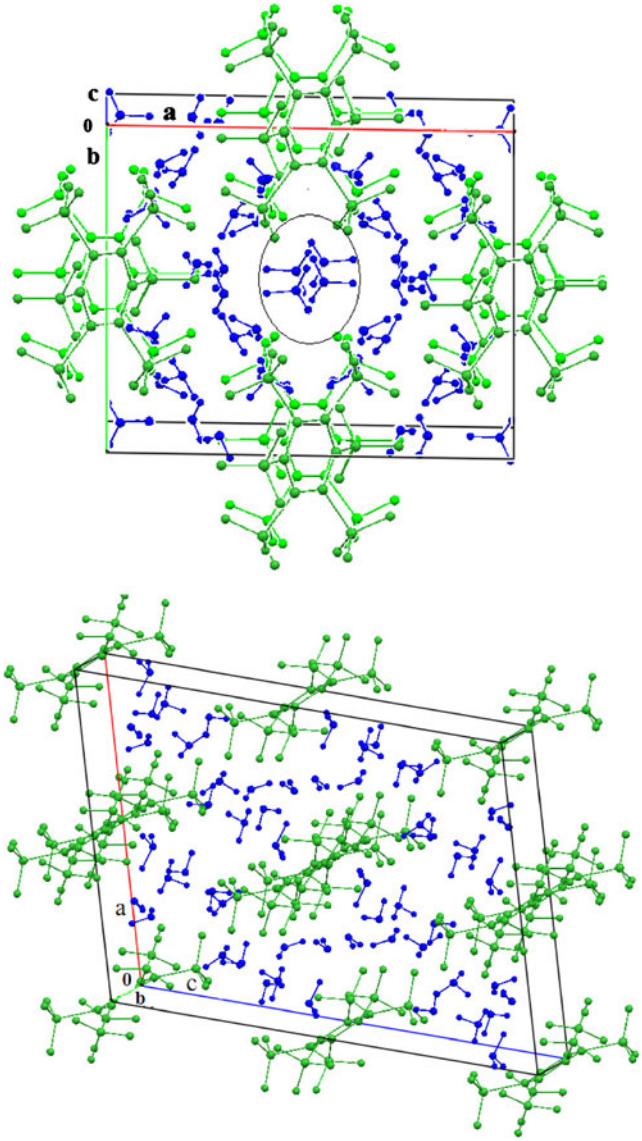

Fig. 3 The crystal structure of BHSA×14H_2O (**2**) in the *c* direction (*top*) showing water channels (the *black ellipse* shows a channel's cross section) and in the *b* direction (*bottom*) showing alternating water and sulfonate (101) layers. $BHSA^{6-}$ anion is marked *green*. H_2O and H_3O^+ are marked *blue*

than the conductivity of samples with 8.1×10^{-4} mol/mol sulfate/BHSA (solid blue circles). This can be rationalized by a model in which the doping protons (balancing the sulfate charge) occupy higher potential energy levels and also have lower energy barriers for proton transport. When a sample with sulfate content of 6.7×10^{-3} mol/mol was heated at 100°C for 20 h, its conductivity increased in time (not shown). Upon cooling to 85°C, the conductivity of the sample was found to be 22 times higher (blue crossed square in Fig. 8) than its value under the same conditions but prior to heating to 100°C. At the same time, the sulfate to benzenesulfonates molar ratio jumped to 0.24 mol/mol. Apparently, heating BHSA above 100°C leads to desulfonation, mostly likely yielding sulfuric and symbenzenetetrasulfonic acids as products [15]. The conductivity of BSHA samples with sulfate/BHSA molar ratio of 3.6×10^{-3} and 8.1×10^{-4} were found to be identical (see Fig. S2), indicating that, at this level, the effect of BHSA doping with sulfuric acid is negligible.

Figure 8 shows that the BHSA conductivity (of the sample with the lowest sulfate content) at constant relative humidity increases with temperature rather uniformly in the whole range of the humidity studied. The activation energy of conductivity ($E_a[\sigma]$=0.24±0.01 eV) does not change much, whereas the preexponential factor, *A*, increases by an order of magnitude, up to 2.6×103 K/Ω cm, as the relative humidity goes from 10% to 50% as shown in Fig. 9.

It is remarkable that, at a given humidity and temperature, the conductivity of *crystalline* BHSA is about the same as the conductivity of Nafion, which relies on proton transfer in *liquid* water retained in sulfonate-clad pores [6]. Due to a low activation energy and preexponential factor of conductivity and because the conductivity vs humidity curve (Fig. 9) does not show plateaus like the water content vs humidity curve (Fig. 1), as expected for bulk protonic conductors [34], one may argue that the high conductivity of BHSA is due to surface water. This question is addressed in the NMR section below.

^{1}H NMR studies of BHSA×12H_2O

The ^{1}H NMR spectra of BHSA×12H_2O powder prepared at 20°C and 9.5% RH are shown in Fig. 10a. With increasing temperature, the line shows pronounced narrowing as shown in Fig. 10b. More detailed lineshape analysis using a fit with two Lorentzians suggests that at room temperature, there are two groups of protons (Fig. 10c): slower (20%) with the linewidth of 31 kHz and faster (80%) with the linewidth of 23 kHz. Upon increasing temperature, the frequency of the fast protons does not change much, but the slow peak moves closer to the position of the fast peak. At the same time, the widths of the peaks decrease with the activation energies of 0.123 eV (slow) and 0.330 eV (fast) (data not shown). At temperatures above 50°C, the two bands merge into a single Lorentzian peak. Its shape, linewidth, and Arrhenius behavior above 50°C (Fig. 10b) suggest that at these temperatures, all protons participate in a common motion which averages out the inter-proton dipole–dipole interaction. The correlation time for this motion, τ_c, can be estimated as follows. The NMR linewidth at half-height $\omega_{1/2}$ for the Lorentzian lineshape is $\omega_{1/2} = 1/(\pi T_2)$, where T_2 is the transverse magnetization relaxation time. In the limit of fast molecular motions ($M_2\ \tau_c << 1$)

$$T_2^{-1} = M_2\tau_c, \text{ or } \tau_c = M_2^{-1}T_2^{-1} = \pi M_2^{-1}\omega_{1/2}, \quad (1)$$

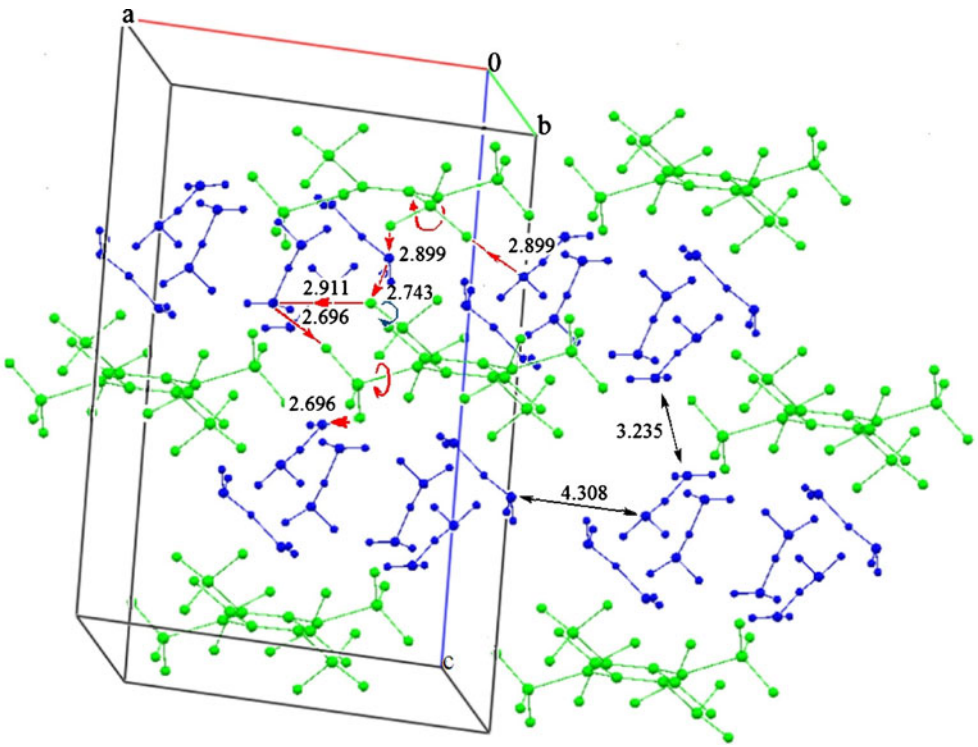

Fig. 4 A view of BHSA×$12H_2O$ off the *a* direction (*a* (0,2), *b* (0,2), *c* (−0.2,0.2)) showing $BHSA^{6-}$ (*green*) layers separated by layers of $H_5O_2^+$ (*blue*) hexamers. O...O distances (in Å) are shown in *black*. *Straight red arrows* show the proposed H^+ translocation path. *Curved red arrows* indicate S–C bond rotations, and *curved blue arrows* indicate S–O bond rotation. Rotations of O–H–O bonds are not shown

where M_2 is the second moment of NMR line when molecular motions are frozen ($\omega_{1/2}$ is in radians per second). This allows one to estimate that, at 75°C, $\tau_c = 1.5\times10^{-6}$s. An Arrhenius fit to the high-temperature part of the dependence in Fig. 10b gives

$$\tau_c = \tau_0 \exp(E_a[T_2]/RT),\ \text{with}\tau_0 = 7.0\ 10^{-10}\text{s},E_a[T_2] = 0.370\text{ev}\ (35.6\text{kJ/mol}) \quad (2)$$

The preexponential factor, $\tau_0=7.0\times10^{-10}$s, is consistent with a simple motion of small molecules [43]. Comparison of $E_a[T_2]$ with typical energies of hydrogen bonds (0.17 eV for water self-diffusivity at room temperature) [34] suggests that the motion requires breaking of about two hydrogen bonds in the rate-limiting step.

Since the BHSA×$12H_2O$ crystals used in this work are rather large (0.1–0.5 mm before caking), the surface water cannot account for a large fraction (80%) of mobile water

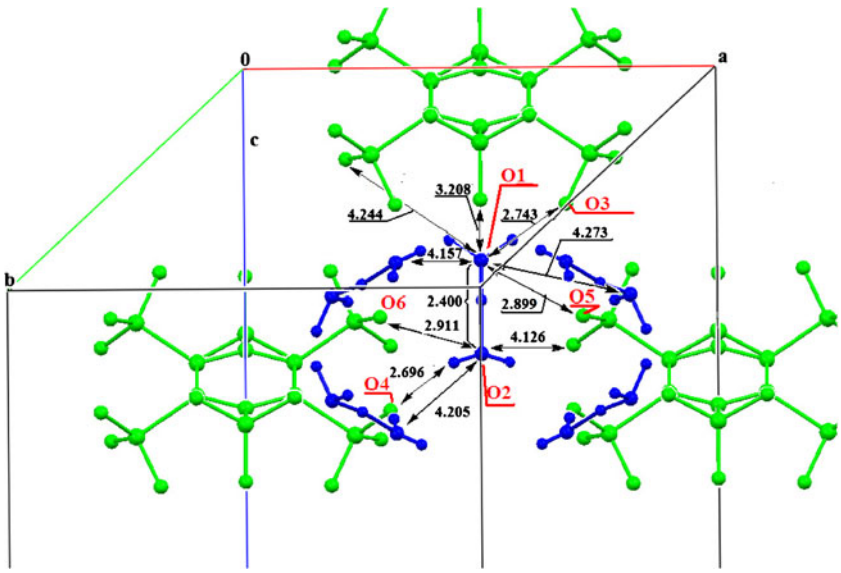

Fig. 5 A view of a Zundel ion in BHSA×$12H_2O$. First and second shell O...O distances (in Å) for one $H_5O_2^+$ ion are shown

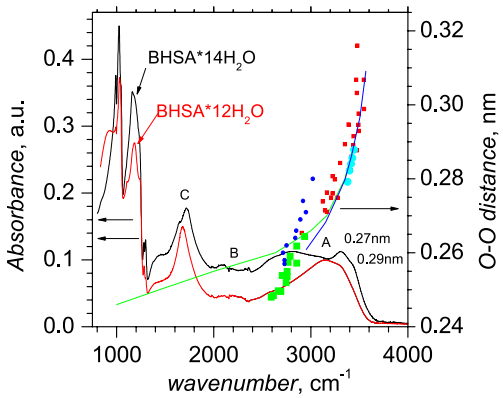

Fig. 6 Mid-IR absorbance spectra of BHSA×12H_2O (*red line*) and BHSA×14H_2O (*black line*) at 21°C. The *right axis* shows experimental and theoretical O...O distances vs O–H vibrational frequencies compiled from literature (symbols: *red* [39], *green* [33], *blue* [38], *cyan* [40]; lines: *green* [37], *blue* [36])

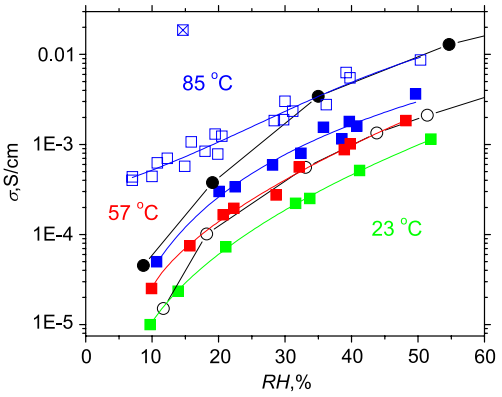

Fig. 8 The dependence of the conductivity of the BHSA powder on relative humidity at 23 (*green*), 57 (*red*), and 85°C (*blue*). *Solid squares* samples with sulfate/BHSA molar ratio of 8.1×10^{-4}, *open squares* 6.7×10^{-3}, and *crossed square* 0.24. Also shown are conductivity data (temperature independent in 23 to 85°C range) for Nafion 950 film (*filled circles*) and Nafion 950 powder (*open circles*). *Solid lines* are fits used in subsequent data analysis

seen at room temperature. Also, fast equilibration between bulk and surface proton populations in the crystal of such size (see proton diffusivity data below) is not likely. Thus, we conclude that none of the two proton populations uncovered by NMR relaxation can be surface water and that both proton populations belong to the bulk. Albeit this is highly speculative at this point, the low temperature limit of the population ratio of slow to fast protons (1:4) may indicate that the slow protons are the central H atoms in the Zundel ions, whereas the fast protons are the four peripheral H atoms of the cations. This conclusion does not rule out the possibility that a small fraction of highly mobile protons (<10% of the total number of protons in the material) in the surface/intergrain regions may lead to large conductivity without showing up as a sharp (Hz wide) ^{1}H NMR peak due to a slow relaxation in their anisotropic environment.

The proton dynamics in BHSA×12H_2O was also studied using ^{1}H NMR T_2 and T_1-relaxation measurements. These measurements yielded conclusions similar to what was drawn from the lineshape analysis presented above, i.e., two types of protons with different relaxation times can be distinguished below 50°C, with the distinction disappearing at higher temperatures. By assuming that jumps translate protons by 0.30 nm, one can estimate the proton diffusion coefficient at 75°C to be $D=6.0\times10^{-10}$cm^2/s (for comparison, the diffusion coefficient in liquid water is 5.0×10^{-5} cm^2/s at 75°C [34] and in DHBNs it is 5×10^{-8}–10^{-6}cm^2/s at 130°C [42]). The estimated diffusion coefficient is at least an order of magnitude too small to be measured with our maximum available gradient strength (60 G/cm). Attempted PFG-NMR diffusivity measurements have been inconclusive.

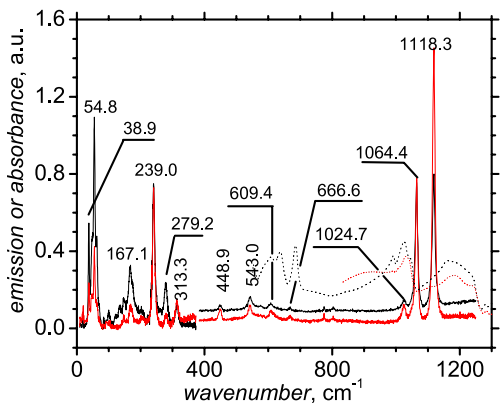

Fig. 7 Raman spectra of BHSA×12H_2O (*red line*) and BHSA×14H_2O (*black line*) at 21°C. Also shown FT IR spectra of BHSA×12H_2O (*red dotted line*) and BHSA×14H_2O (*black dotted line*)

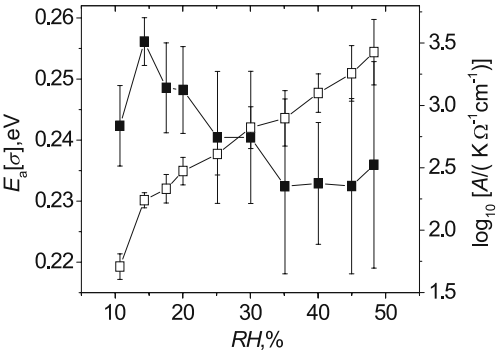

Fig. 9 Dependence of the activation energy ($E_a[\sigma]$, *filled squares*) and the preexponential factor (A, *open squares*) of BHSA conductivity on relative humidity. E_a and A were found from equation $\ln(\sigma T)=\ln A+E_a[\sigma]/(RT)$. *Error bars* represent the standard deviations of the fitting parameters of the Arrhenius lines at constant humidities (see Fig. S3)

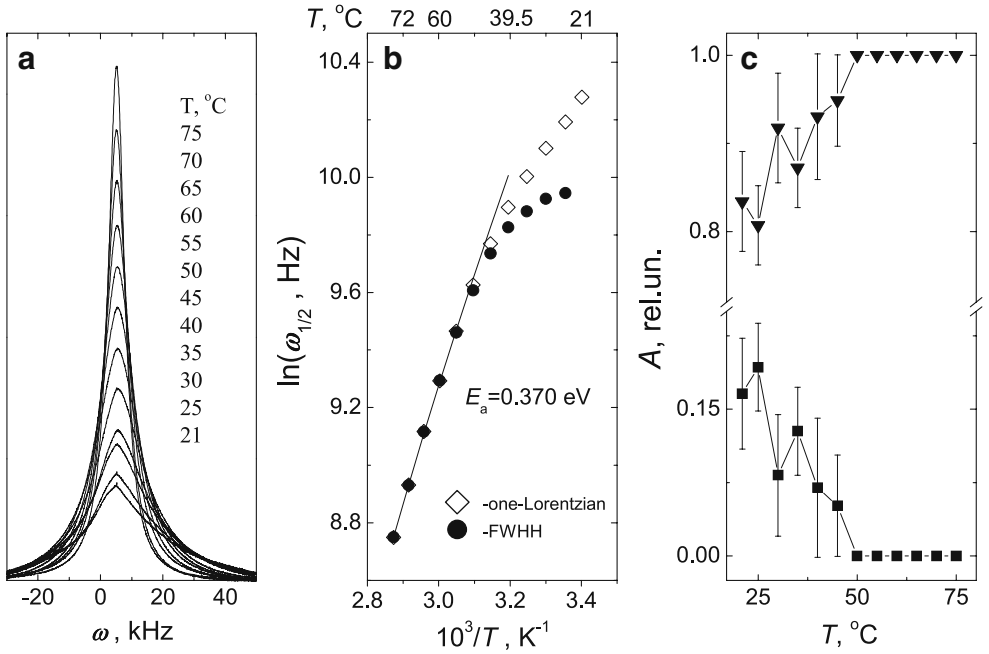

Fig. 10 **a** ^{1}H NMR spectra (single $\pi/2$ pulse) of BHSA×$12H_2O$ powder at different temperatures. $T = 21, 25, 30, 35, 40, 45, 50, 55, 60, 65, 70, 75$°C. Zero frequency corresponds to ^{1}H resonance in tetramethylsilane. **b** Arrhenius plot of the temperature dependence of full width at half-height (*FWHH*) and of the linewidth parameter from a single Lorentzian fit of the data in **a**. **c** Normalized peak areas of the two Lorentzian peaks used in fitting data in **a**

Discussion

The low values of activation enthalpy of conductivity in BHSA×$12H_2O$ and BHSA×$14H_2O$ (0.24±0.01 eV) are similar to 0.26±0.03 eV found in materials with disordered hydrogen-bonded networks (DHBN, such as $CsHSO_4$), which correspond to the O...O distances of 0.265 nm [42] (or 0.27–0.29 nm) [34] and are optimal for both proton translocation and OH rotation. Furthermore, the preexponential factor, A, is on the order of 103 K/Ω cm, i.e., the same as in DHBNs [42]. The weak dependence of the activation energy of conductivity on humidity, the strong increase of the conductivity of BHSA with the concentration of extrinsic protons (H_2SO_4 doping), and the multiple vacant proton positions in its structure are in favor of viewing BHSA as a bulk conductor with a disordered protonic sublattice.

On the other hand, the Arrhenius parameters of conductivity are also consistent with the values found for hydrous oxides such as $Sb_2O_5 \times xH_2O$ and zirconium phosphates, for which liquid-like surface conductivity has been proposed [34]. The strong increase of the conductivity preexponential Arrhenius factor of BHSA with humidity, the 1.5 times smaller activation energy of conductivity compared with the activation energy of T_2 relaxation, and the fact that no inflections in conductivity parameters are observed at 20% humidity (when the crystal structure changes) or at 50°C (when NMR shows exchange of all bulk protons in the μs timescale) support the occurrence of surface protonic conductivity in BHSA.

The bulk conductivity model provides an estimate of the conductivity, σ, of BHSA×$12H_2O$ on the basis of the Nernst–Einstein equation. Assuming all protons being mobile,

$$\sigma = \frac{DCe^2}{kT}$$
$$= \frac{6.0 \cdot 10^{-10}\,\mathrm{cm}^2/s \times 4.176 \cdot 10^{22}\,\mathrm{cm}^{-3} \times \left(1.60 \cdot 10^{-19} C\right)^2}{1.38 \cdot 10^{-23}\,\mathrm{J}/K \times 348\,\mathrm{K}}$$
$$= 1.3 \cdot 10^{-4}\,\mathrm{S/cm}$$

where the proton diffusion coefficient $D = 6.0 \times 10^{-10}\,\mathrm{cm}^2/\mathrm{s}$ (from T_2 at 75°C), the total proton concentration in BHSA×$12H_2O$ $C = 4.176 \cdot 10^{22}\,\mathrm{cm}^{-3} = 69.4\,\mathrm{M}$ (from XRD). The calculated conductivity is in reasonable agreement with the experimental value, 3.9×10^{-5} S/cm, interpolated to 75°C and 10% RH from the data in Fig. 8. From the viewpoint of the surface conductivity model, this agreement is likely to be coincidental; the true concentration of mobile protons can be smaller, and their diffusivity can be larger. Although further studies are needed to determine more detailed nature of its protonic conductivity, we can ascertain now that BHSA should be classified as a fast protonic conductor based on the conductivity and the activation energy criteria proposed earlier [34].

It is interesting to compare the conductivity of the BHSA (DOS=6) with the conductivity of polyphenylenesulfide (DOS=0.7) studied earlier in our laboratory [44]. In the 50–85°C range and at humidities below 30%, the polymer

shows conductivity comparable with BHSA despite the lower concentration of protons. This may be due to the amorphous nature of the polymer, which creates low activation energy ($E_a[\sigma]$=0.15 eV) pathways [44] for protons unavailable in purely crystalline materials.

Conclusions

Our data on the conductivity of benzenehexasulfonic acid in a wide range of temperature, humidity, and sulfuric acid dopant concentration suggest that this material is a fast protonic conductor with the behavior showing signs of both surface and bulk conductivity. NMR relaxation studies of BHSA×12H_2O reveals the existence of two types of bulk protons, which undergo exchange on the μs time scale above 50°C. We tentatively assign these two proton populations to inner and outer protons in Zundel ions. For some materials, a crystalline phase with a disorder in the ionic sublattice shows higher conductivity than corresponding amorphous phases. This situation does not seem to apply to our case since the intergrain conductivity appears to overwhelm the bulk conductivity in BHSA. The fact that the conductivity of the amorphous polyphelynele-sulfide with a low degree of sulfonation is comparable with the conductivity of a crystalline material with a high degree of sulfonation suggests that the amorphous phases are responsible for conductivity of BSHA and sulfonated polyphenylenes. The results of this work show that fast protonic conductivity is possible in crystalline highly sulfonated materials, which retain crystallization water at low humidities. More amorphous and defective highly sulfonated aromatic polymers, of which BHSA is a prototype, can be expected to achieve low-humidity protonic conductivity significantly larger than BHSA or Nafion as was shown recently by Litt and coworkers [11, 12].

Acknowledgment The funding for this work was provided by the US Department of Energy, US National Science Foundation, Ohio Department of Development, Farris Family Innovation Fund and Kent State University.

References

1. Gasteiger HA, Mathias MF (2002) Fundamental research and development challenges in polymer electrolyte fuel cell technology. Proton conducting membrane fuel cells III symposium. Electrochemical Society, Salt Lake City
2. Savadogo O (2004) Emerging membranes for electrochemical systems—part II. High temperature composite membranes for polymer electrolyte fuel cell (PEFC) applications. J Power Sources 127:135–161
3. Hogarth WHJ, da Costa JCD, Lu GQ (2005) Solid acid membranes for high temperature (>140 °C) proton exchange membrane fuel cells. J Power Sources 142:223–237
4. Kreuer KD (2000) On the complexity of proton conduction phenomena. Solid State Ion 136:149–160
5. Schuster M, Rager T, Noda A, Kreuer KD, Maier J (2005) About the choice of the protogenic group in PEM separator materials for intermediate temperature, low humidity operation: a critical comparison of sulfonic acid, phosphonic acid and imidazole functionalized model compounds. Fuel Cells 5:355–365
6. Doyle M, Rajendran G (2003) Perfluorinated membranes. In: Vielstich W, Lamm A, Gasteiger H (eds) Handbook of fuel cells: fundamentals, technology and applications. Wiley, New York, pp 352–395
7. Khiterer M, Loy DA, Cornelius CJ, Fujimoto CH, Small JH, McIntire TM, Shea KJ (2006) Hybrid polyelectrolyte materials for fuel cell applications: design, synthesis, and evaluation of proton-conducting bridged polysilsesquioxanes. Chem Mater 18:3665–3673
8. Rikukawa M, Sanui K (2000) Proton-conducting polymer electrolyte membranes based on hydrocarbon polymers. Prog Polym Sci 25:1463–1502
9. Alberti G, Casciola M, Massinelli L, Bauer B (2001) Polymeric proton conducting membranes for medium temperature fuel cells (110–160°C). J Membr Sci 185:73–81
10. Miyatake K, Shouji E, Yamamoto K, Tsuchida E (1997) Synthesis and proton conductivity of highly sulfonated poly(thiophenylene). Macromolecules 30:2941–2946
11. Granados-Focil S, Litt MH (2004) New class of polyelectrolytes, polyphenylene sulfonic acids and its copolymers, as proton exchange membranes for PEMFC's. Abstracts of Papers of the American Chemical Society 228:U657–U657
12. Kang J (2008) A new class of polyelectrolyte; poly(*p*-phenylene disulfonic acids) macromolecular science and engineering dissertation case. Western Reserve University, Cleveland, OH, p 313
13. Taninouchi Y, Hatada N, Uda T, Awakura Y (2009) Phase relationship of CsH_2PO_4–$CsPO_3$ system and electrical properties of $CsPO_3$. J Electrochem Soc 156:B572–B579
14. Dokunikhin NS, Gaeva LA, Mezentseva GA (1972) Benzenehexasulfonic acid. Dokl Akad Nauk SSSR 206:624–626
15. Dokunikhin NS, Mezentseva GA (1976) Higher polysulfonic acids of benzene. Zhurnal Organicheskoi Khimii 12:621–625
16. Khmelnitskaya EY, Mezentseva GA, Dokunikhin NS (1980) Electrochemical reduction of benzene hexasulfonic, pentasulfonic, and tetrasulfonic acids. Sov Electrochem 16:940–945
17. Maksimov YM, Cheshchevoi VN, Podlovchenko BI (1985) Effect of the structures of aromatic sulfonic acids on their adsorption at platinum electrodes. Vestnik Moskovskogo Universiteta, Seriya 2: Khimiya 26:477–479
18. Chetkina LA, Sobolev AN, Mezentseva GA, Dokunikhin NS (1975) Structure of crystals of octahydrate of hexasodium salt of benzenehexasulfonic acid. Doklady AN SSSR 220:1343–1346
19. Chetkina LA, Sobolev AN (1977) The crystal structure of the hexasodium salt of benzenehaxasulfonic acid octahydrate. Acta Cryst B 33:2751–2756
20. Berckmans VSF, Holleman AF (1925) The tetrachloronitrobenzenes, the tetrachlorodinitrobenzenes; their reaction with sodium methylate. Anales Soc Espan Fis Quim 23:358–371
21. Garanin EM, Tolmachev YV (2008) Apparatus for measurement of protonic conductivity of powdered materials as a function of temperature and humidity. J Electrochem Soc 155:B1251–B1254
22. March J (1992) Advanced organic chemistry, 4th edn. Wiley, New York
23. Garanin EM, Tolmachev YV, Hoover RR, Adas S, Bunge SD, Gangoda M, Khitrin AK, Woods S, Malkovskiy A, Solak N,

Wesdemiotis C (2010) Stability and tautomerization of cyclic anhydrides of benzenehexasulfonic acid. J Org Chem (in press)
24. Collard DM, Sadri MJ, Vanderveer D, Hagen KS (1995) Highly twisted substituted Arenes—X-ray structure and dynamic H-NMR spectra of 1, 4-dialkyl-2, 3, 5, 6-tetrakis(alkylsulfonyl)benzenes. J Chem Soc Chem Commun 1995:1357–1358
25. Attig R (1976) Cryst Struct Commun 5:223
26. Attig R, Mootz D (1976) Acta Cryst B 32:435
27. Lundgren JO (1972) Acta Cryst B 28:1684
28. Skakle JMS, Wardell JL (2006) Acta Cryst E 62:o1402
29. Devlin JP, Severson MW, Mohamed F, Sadlej J, Buch V, Parrinello M (2005) Experimental and computational study of isotopic effects within the Zundel ion. Chem Phys Lett 408:439–444
30. Koleva V, Stefov V, Cahil A, Najdoski M, Soptrajanov B, Engelen B, Lutz HD (2009) Infrared and Raman studies of manganese dihydrogen phosphate dihydrate, $Mn(H_2PO_4)_2x2H_2O$. Part II: region of the internal OH group vibrations. J Mol Struct 919:164–169.
31. Zarubin DP (1999) Infrared spectra of hydrogen bonded hydroxyl groups in silicate glasses. A re-interpretation. Phys Chem Glasses 40:184–192
32. Baumer U, Boldt K, Engelen B, Muller H, Unterderweide K (1999) Preparation, crystal structure and IR spectra of $BeSeO_3$ x H_2O–hydrogen bonds and correlation of IR and structure data in the monohydrates $MSeO_3$ x H_2O (M=Be, Ca, Mn, Co, Ni, Zn, Cd). Zeitschrift Fur Anorganische Und Allgemeine Chemie 625:395–401
33. Choi BK, Lee MN, Kim JJ (1989) Raman-spectra of the NaH_2PO_4 crystal. J Raman Spectrosc 20:11–15
34. Colomban P (1992) Proton conductors: solids, membranes and gels—materials and devices. Chemistry of solid state materials. Cambridge University Press, Cambridge, p 581
35. Lutz HD (2003) Structure and strength of hydrogen bonds in inorganic solids. J Mol Struct 646:227–236
36. Mikenda W (1986) Stretching frequency versus bond distance correlation of O–D(H)...Y (Y=N, O, S, Se, Cl, Br, I) hydrogen bonds in solid hydrates. J Mol Struct 147:1–15
37. Novak A (1974) Hydrogen bonding in solids. Correlation of spectroscopic and crystallographic data. In: Dunitz JD (ed) Structure and bonding. Springer, Berlin, pp 117–216
38. Unterderweide K, Engelen B, Boldt K (1994) Strong hydrogen-bonds in acid selenites—correlation of infrared spectroscopic and structural data. J Mol Struct 322:233–239
39. Hermansson K, Gajewski G, Mitev PD (2008) Pressure-induced OH frequency downshift in Brucite: frequency–distance and frequency field correlations. J Phys Conf Ser 117:012018
40. Bratos S, Leicknam JC, Pommeret S (2009) Time-resolved infrared spectroscopy of water. Relation between the OH stretching frequency and the O-O distance. Pol J Chem 83:737–745
41. Bomann D, Tilloy S, Monflier E (1999) Comparative Raman spectroscopy study of sulfonate-substituted triphenylphosphines. Vibr Spectrosc 20:165–172
42. Baranov AI (2003) Crystals with disordered hydrogen-bond networks and superprotonic conductivity. Review. Crystallogr Rep 48:1012–1037
43. Moller H, Mullerwarmuth W, Ruschendorf F, Schollhorn R (1987) Zeitschrift Fur Physikalische Chemie Neue Folge 151:121–131
44. Garanin EM, Towers MS, Toothaker PW, Laali K, Tolmachev YV (2010) Conductivity of highly sulfonated polyphenylene sulfide in the powder form as a function of temperature and humidity. Polymer Bull 64:595–605